Hindawi
Mobile Information Systems
Volume 2023, Article ID 9829310, 1 page
https://doi.org/10.1155/2023/9829310

Retraction

Retracted: Regular Flow Field Sparse Processing and Blue Finance of Ocean City Research Based on GIS System

Mobile Information Systems

Received 31 October 2023; Accepted 31 October 2023; Published 1 November 2023

This article has been retracted by Hindawi following an investigation undertaken by the publisher [1]. This investigation has uncovered evidence of one or more of the following indicators of systematic manipulation of the publication process:

(1) Discrepancies in scope

(2) Discrepancies in the description of the research reported

(3) Discrepancies between the availability of data and the research described

(4) Inappropriate citations

(5) Incoherent, meaningless and/or irrelevant content included in the article

(6) Peer-review manipulation

The presence of these indicators undermines our confidence in the integrity of the article's content and we cannot, therefore, vouch for its reliability. Please note that this notice is intended solely to alert readers that the content of this article is unreliable. We have not investigated whether authors were aware of or involved in the systematic manipulation of the publication process.

Wiley and Hindawi regrets that the usual quality checks did not identify these issues before publication and have since put additional measures in place to safeguard research integrity.

We wish to credit our own Research Integrity and Research Publishing teams and anonymous and named external researchers and research integrity experts for contributing to this investigation.

The corresponding author, as the representative of all authors, has been given the opportunity to register their agreement or disagreement to this retraction. We have kept a record of any response received.

References

[1] Y. Sun and K. Anurag, "Regular Flow Field Sparse Processing and Blue Finance of Ocean City Research Based on GIS System," *Mobile Information Systems*, vol. 2022, Article ID 7650704, 10 pages, 2022.

Hindawi
Mobile Information Systems
Volume 2022, Article ID 7650704, 10 pages
https://doi.org/10.1155/2022/7650704

Research Article

Regular Flow Field Sparse Processing and Blue Finance of Ocean City Research Based on GIS System

Ying Sun[1] **and Kalra Anurag**[2]

[1]*Yantai University of Science and Technology, Shandong 430074, China*
[2]*Ecological and Environmental Research Center, Kyrgyz-Turkish Manas University, Bishkek, Kyrgyzstan*

Correspondence should be addressed to Kalra Anurag; anurag@email.cu.edu.kg

Received 3 June 2022; Revised 20 July 2022; Accepted 28 July 2022; Published 24 August 2022

Academic Editor: Chi Lin

In order to explore the development path of blue finance in ocean cities, this paper combines GIS to conduct blue finance research in ocean cities, draws on the traditional direct visualization method of point icons, and uses arrow symbols to render vector flow field data. Moreover, this paper uses GIS means to perform statistical analysis on flow field data, studies the adaptive sparse algorithm of flow field data spatial structure based on GIS, and proposes a program implementation method for regular flow field sparse processing suitable for the general flow of the sparse algorithm. The experimental research shows that the GIS technology proposed in this paper can play an important role in the research of blue finance in ocean cities and has a certain role in promoting the development of ocean blue finance.

1. Introduction

The development of the world economy shows that the coastal areas have become the regions with the most concentrated population, the highest degree of urbanization, and the most developed economy. The coastal areas of the world are about more than 2/3 of the world's population, and 60% of the large and medium cities are distributed. China is one of the major maritime countries in the world, and most of the developed cities are concentrated in the coastal areas. Among them, the coastal area, which accounts for 15% of the country's land area, carries more than 40% of the country's population, 50% of large and medium-sized cities, and 60% of its GDP.

The ocean industry is the production and service activities carried out by human beings to develop, utilize, and protect the ocean and refers to the sum of various material production and nonmaterial production sectors formed by human development, utilization, and protection of ocean resources. That is, it is the various production and service activities carried out by human beings using ocean resources and ocean space, or the social production, exchange, distribution, and consumption activities of human beings in the ocean and targeting ocean resources [1].

Finance is the engine of economic development, and the level of financial development will directly affect the degree of economic development [2]. At present, the continuous development of financial globalization, the continuous enhancement of international capital mobility, and the continuous increase of mergers and reorganizations of financial institutions have undoubtedly exacerbated the phenomenon that financial activities, financial factors, and financial institutions are highly concentrated in some large financial centers [3]. At present, the three most eye-catching international financial agglomeration areas are New York, Tokyo, and London. Beijing Financial Street and Shanghai Lujiazui agglomeration area are currently formed and basically perfected financial agglomeration areas in China. Qingdao, as the vanguard of the blue economic zone in Shandong Peninsula, has formulated a development plan for building a regional financial center in order to realize the blue leap. This era is not only an era led by science and technology, but also an era of soaring oceans. With the emergence of resource crisis, people's attention is once again focused on the ocean.

Therefore, exploring the treasures of the ocean and finding development forces from the ocean have become the new direction for the economic development of various countries.

The ocean economic theory is an important part of the blue economic theory. Before the twentieth century, restricted by the level of technology, the development and utilization of marine resources could only stay at the surface—fishing, salt production, sea transportation, etc. Later, with the progress and innovation of technology, people gradually began to explore the development and utilization of marine resources. The term "ocean economy" was first proposed in the United States in the early 1970s. As population growth put a heavy pressure on land resources, some developed countries began to formulate some marine development plans and invested a lot of capital into them.

Marine economy is a general term for marine activities carried out by all marine-related industrial sectors in a country or a region to develop or utilize marine resources. Its essence is activities related to marine resources, and it has two characteristics of comprehensiveness and sea-related. After the continuous development of traditional marine activities, a marine economy in the modern sense has been formed. The marine economy in the modern sense is a collective economic concept, including not only productive activities for scientific and technological development of marine resources and expansion of marine space, but also service activities that provide support for marine development and space expansion.

This paper combines the GIS to carry out the research on the blue finance of the ocean city, to improve the exploration effect of the blue finance of the ocean city, and to provide a theoretical reference for the further development of the blue finance of the ocean city.

2. Related Work

Marine Geographic Information System (MGIS) is a combination of geographic information system technology and marine science and applications. The application of GIS in the marine field can be traced back to the marine automation carried out by the National Ocean Survey (NOS) in the 1960s. However, some initial researchers simply applied GIS directly to the management of the marine environment. Literature [4] designed a sharing service system for marine stereoscopic monitoring data based on distributed database, WebGIS, and other technologies and elaborated in detail. The data organization structure, overall framework, business function modules, and implementation methods of spatial data publishing and services are adopted by the shared service system.

Literature [5] studies the preliminary application of GIS in coastal zone management. Try to explore the application of GIS in coastal environment. Literature [6] affirmed the importance of GIS in managing and displaying marine data and also discussed the three-dimensional modeling, visualization, and quantitative analysis of marine data. Literature [7] proposed the spatial structure of marine GIS and spatial simulation integration. Literature [8] conducted in-depth research on the expression, analysis, and visualization of marine data. Literature [9] combines JavaJJava3d, visualization toolkit, and ESRI's ArcGIS Engine to build a GIS prototype system including ocean models. Through ArcGIS Engine's spatial analysis capabilities and Java3D's complex visualization capabilities, users can input data and perform spatial and scientific analysis and virtual visualization of the output results. Literature [10] advocated the research and development of coastal and marine GIS and put forward the concept of "global database with coastal chain as the baseline." Literature [11] combined GIS and tidal current model to study tidal wave system. Literature [12] studied and analyzed the visualization of tidal current numerical simulation from the perspective of geographic information system and designed and implemented a virtual reality prototype of coastal ocean current simulation. On the basis of analyzing the advantages and disadvantages of various data models, literature [13] proposed a three-dimensional GIS data model and a marine spatiotemporal data model suitable for marine information management. Literature [14] takes the multisource, multidimensional, and dynamic massive data of coastal zones and oceans as the research object and designs a GIS spatial data model for marine data to realize the unified management and expression of multisource, multidimensional, and massive data, especially the three-dimensional dynamic expression. Literature [15] uses GIS technology to study the management and visualization methods of marine hydrological data. Based on the spatial location management of hydrological data, the visual expression of hydrological data is realized in the form of vector graphics and statistical histograms, and GIS visualization tools are used to detect the seabed. The data is managed, and the spatial visualization relationship between the profile data and the planar distribution data is established, which provides a shortcut for the visualization of seabed scientific research. Literature [16] established a seabed sediment visualization simulation environment by establishing a marine sediment database. Based on bathymetry data, multibeam data, borehole data, and stratigraphic trawl samples, a three-dimensional visualization simulation system for the seabed was built. On the basis of analyzing the demand for information expression of digital ocean water elements, literature [17] proposed a water cube liter data model and its establishment method and realized the simulation of sea surface, the three-dimensional expression of water elements, and the construction of virtual ocean scenes. Literature [18],considering the combination of geographic information system and virtual reality technology, uses multisource and heterogeneous basic data to establish a realistic and dynamic three-dimensional virtual ocean environment and visualize the observation data in the virtual ocean. With the development of network technology, WebGIS is used in marine science. The application research of marine information is also more and more extensive. Literature [19] analyzed the development of marine basic geographic basemap for marine information sharing and the implementation of marine information WebGIS and realized the sharing of marine information and hazards based on WebGIS. In literature [20], aiming at the shortcomings of the existing WebGIS in

the field of marine information sharing, a method based on Spatial Database Engine (SDE) to manage marine remote sensing data is proposed, thus realizing the marine remote sensing WebGIS oriented to the distributed heterogeneous database environment.

3. GIS Visualization Technology Analysis of Flow Field

GIS stores spatial data in the form of layers, the flow field is multitime data, and each time data is a vector layer. These layers are integrated into a layer group (Group Layer), which is convenient for data management and observation and analysis of flow field motion in time series. Therefore, when rendering the flow field, a uniform flow velocity threshold and the length and color of the corresponding rendering symbols should be specified. However, observing the data, it can be found that the numerical distribution range of the data velocity at different times is very different. Figure 1 shows the numerical distribution characteristics of the flow velocity at the first and 72nd time during the storm surge. The value distribution at the first time is between 0 and 0.1, while the range at the 72nd time is between 0 and 1.5.

If the data is rendered linearly, the spatial characteristics of the flow velocity cannot be highlighted. Therefore, in order to enhance the contrast effect of the flow field, in this paper, when the flow field is uniformly rendered, the symbol length and symbol color are processed, and the flow field is rendered nonlinearly.

3.1. Length Map Rendering. The flow field data is rendered with arrow symbols, and the length of the arrow indicates the magnitude of the flow velocity. Since the change of the flow field is a dynamic process in a long-term sequence, when rendering the data at each moment, the maximum value of the flow velocity at all moments should be uniformly selected as the upper limit of the rendering. In this paper, the maximum velocity range of the Jiaozhou Gulf flow field at multiple times is about 1.5. When the symbol length is linearly corresponding to the velocity value, the formula is as follows:

$$size = \left(V \div V_{\max}\right) \times 1000. \tag{1}$$

In the formula, $V_{\max}$ represents the flow rate, g is the maximum flow rate, and the maximum value of the symbol length corresponding to the maximum flow rate is 1000. However, since the numerical ranges of the flow velocity in the flow field at different times are different, the spatial distribution of the flow velocity in the flow field at the same time is not uniform.

In order to avoid this problem and highlight the numerical variation characteristics of most elements, it is necessary to set the symbol length within an appropriate range according to certain rules. This paper nonlinearly maps the symbol size to between 70 and 600, as shown in Figure 2.

The formula for nonlinear mapping is as follows:

$$aftersize = \begin{cases} size \in (0, 70), \\ size, size \in (70, 500), \\ 500 + (size - 500) \times 0.2. \end{cases} \tag{2}$$

In the formula, aftersize is the symbol size after nonlinear mapping, and size is the size of linear mapping.

Figure 3 shows the comparison of the effect of general linear mapping and nonlinear mapping of symbol length in the same region of the flow field. Although the vortex characteristics of the water flow can be seen in both Figures 3(a) and 3(b), the symbols of the general linear mapping have little difference in the length of the vortex, which cannot reflect the changing law of the water flow velocity at the vortex. However, Figure 3(b) clearly shows that the flow velocity in the center of the vortex is small, and the flow velocity increases toward the outside.

3.2. Color Stretching Rendering. In flow field rendering, the color stretching of symbols is also a way to express the magnitude of the flow velocity. The color stretching of the flow field, that is, the rendering of the color by subshort, is to divide the elements of the flow field into several segments according to the flow rate and then select a starting color and an ending color to form a color band. Finally, the corresponding relationship between the flow velocity of each segment and the color on the ribbon is established according to certain rules, and the arrow symbols of the flow field elements at each level are rendered into corresponding colors.

The formula for nonlinear mapping is as follows:

$$colorin\ de\ x = \begin{cases} breakvalue \times 140, breakvalue \in [0, 1], \\ breakvalue \times 20 + 140, breakvalue \in [1, 1.5]. \end{cases} \tag{3}$$

In the formula, breakvalue is the flow velocity value of the flow field element, and colorindex is the index number of the color block corresponding to the color ribbon.

Figure 4 shows the comparison of the effect before and after the nonlinear mapping of the flow field symbol color. Figure 4(a) is a single-color map, and the color of the flow field symbol does not change. Figure 4(b) is a nonlinear color mapping. With the change of the flow rate, the color of the flow field symbol also changes, and the expression of the seawater flow law is more vivid.

Figure 5 depicts the relationship between map scale and flow field feature display. As the scale is reduced, the size of the spatially fixed features on the map is smaller. However, the size of the computer screen is fixed, which results in a large number of features on a small-scale map and a small distance between features.

The degree of sparseness of the data is related to the cell size of the grid used to control the display of features. To achieve adaptive sparsification, the size of grid cells should change with the scale. It can be seen from Figure 6 that when browsing the map in a large scale at a small scale, the grids with larger unit size (smaller number) are used for thinning. At this time, the level of detail of the data is lower; that is, the

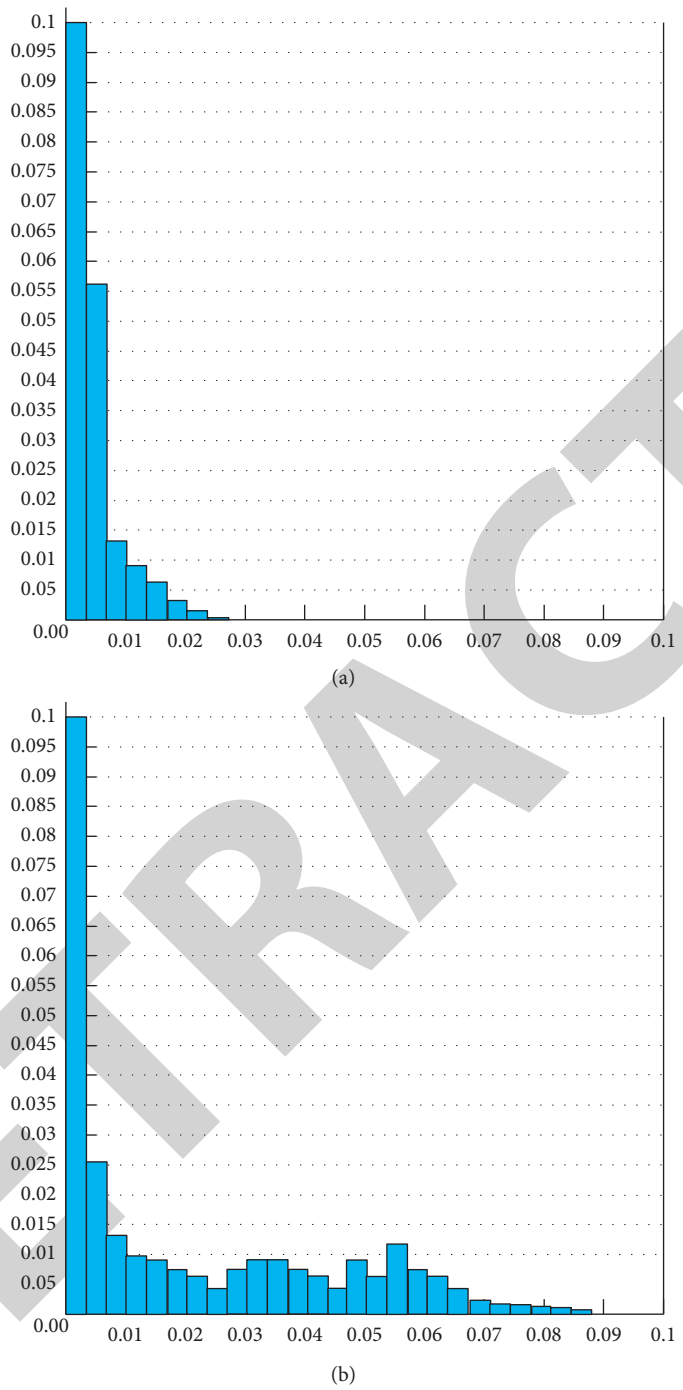

Figure 1: Numerical distribution characteristics of flow velocity. (a) The first moment. (b) The 72nd moment.

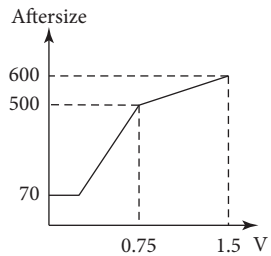

Figure 2: Nonlinear mapping of symbol length.

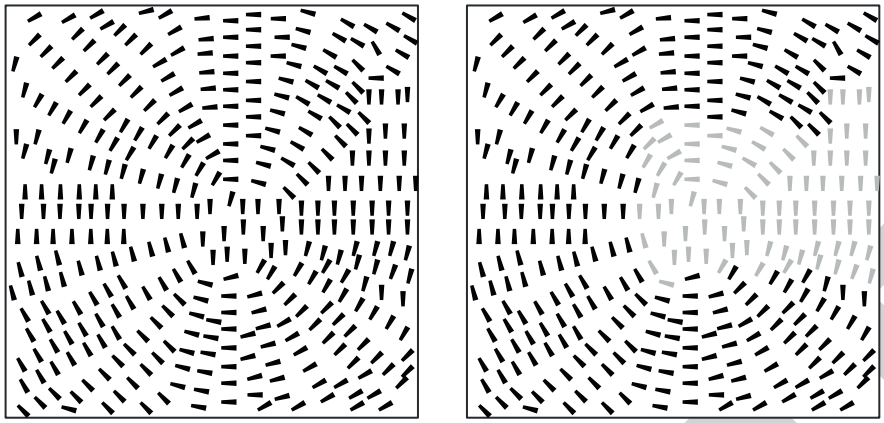

(a) (b)

Figure 3: Comparison of flow field symbol length mapping effects. (a) General linear mapping. (b) Nonlinear mapping.

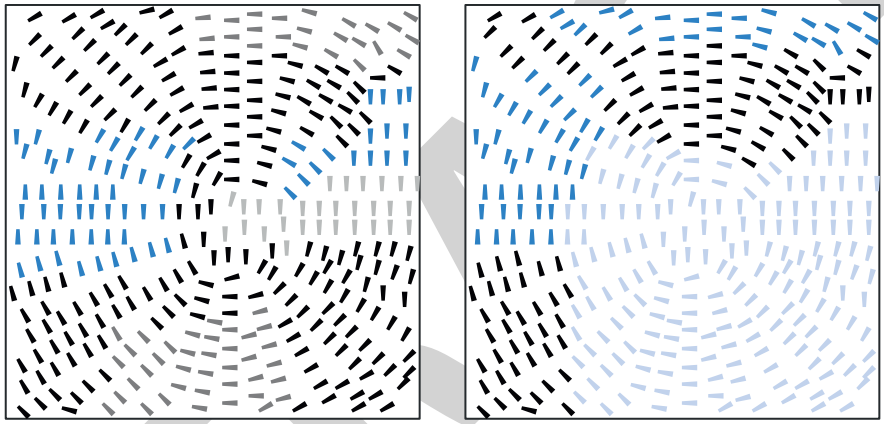

(a) (b)

Figure 4: The rendering before and after nonlinear color mapping. (a) Single-color mapping. (b) Nonlinear mapping.

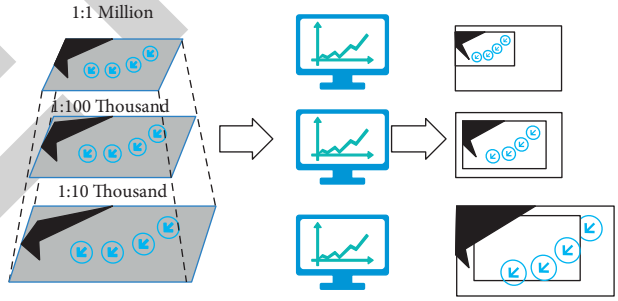

Figure 5: The relationship between map scale and element display.

degree of sparseness is higher. When viewing in a large scale and a small area, that is, when the map is enlarged, in order to highlight the details of the flow field and display more elements, a grid with a smaller unit size (more number) is used for thinning. At this time, the data display has a higher level of detail, that is, a lower degree of sparseness, as shown in Figure 6.

Therefore, the adaptive thinning processing is divided into the following steps: determining the scale range of the adaptive processing, the scale classification, and the calculation of the grid size at each level. Finally, an adaptively processed grading table is obtained, and the scale and grid size of each level are recorded.

To realize the adaptive sparse processing of the flow field, the key step is to determine the relationship between the map scale and the grid size. This paper calculates that, for the flow field data with specific spatial distribution (element range, element location), the distance between the displayed elements at any scale should be kept the same. Then, there is a constant relationship between the scale and the size of the

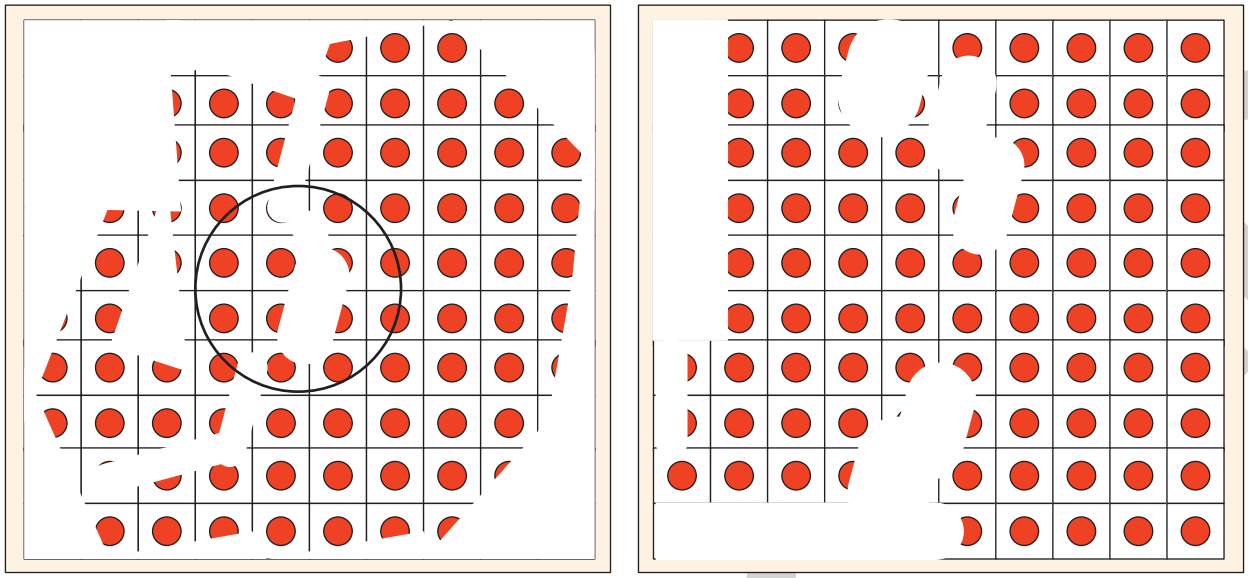

(a) (b)

Figure 6: Grid size at different scales. (a) Grid size at 1 : 60,000. (b) Grid size at 1 : 22,000.

corresponding grid, which is defined as the spatial density eigenvalue in this paper. It can be seen that the spatial density eigenvalue is an important parameter to describe the relationship between flow field sparse processing and scale.

First, we define several variables: width represents the real spatial width of the ocean field, and L represents the width of the computer screen that displays the ocean field. num represents the number of points in a single direction (here, the horizontal direction is used as an example) within the screen range after thinning, and space is the point interval. As mentioned above, the empirical value is space e [1.8, 2.3 cm].

This paper selects any two display levels to analyze the relationship between scale and grid number. We set these two grid levels as i, j. Under the level i, the corresponding scale is S_i, the actual space width of the screen coverage is L_i, and the number of horizontal grids of the matching grid is N_i. Under the j level, the corresponding scale is S_j, the actual space width of the screen coverage is L_j, and the grid number of the matching grid is N_j, as shown in Figure 7.

Since the scale bar = distance on the map/distance on the ground, such as 1/5,000, means that 1 meter on the map represents the distance on the ground of 5 kilometers, we obtain

$$S_i = L/L_i, \tag{4}$$

$$S_j = L/L_j. \tag{5}$$

Since the number of points displayed on the current screen is fixed and the real width of the current screen = the real width of the point interval $*$ the number of points, we obtain

$$L_i = wi\ dt\ h/N_i \times num, \tag{6}$$

$$L_j = wi\ dt\ h/N_j \times num. \tag{7}$$

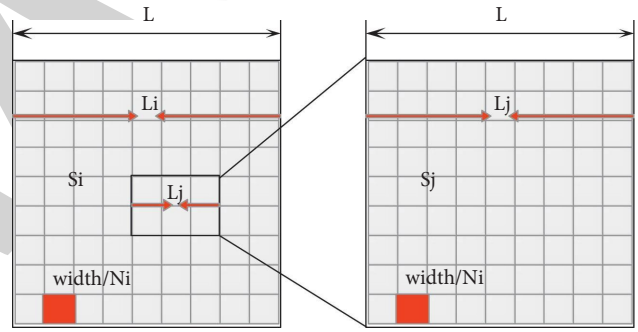

Figure 7: Quantitative relationship under any two display levels.

From formulas (1)–(4), the following is calculated:

$$N_i/S_i = N_j/S_j = num \times wi\ dt\ h/L = \lambda. \tag{8}$$

It can be seen from formula (8) that the ratio of the number of grids at any level to the corresponding scale is a constant. In this paper, this number is defined as the eigenvalue of the spatial density of the massive field, and formula (8) is called the eigenvalue formula. Based on the characteristics of this formula, the number of cells and corresponding scales of grids at each level can be calculated.

According to the relationship between the number of grids and the scale obtained above, it can be seen that the number of grids corresponding to each level of scale can be calculated only by the spatial density characteristic value of the massive field, and vice versa, and the display scale corresponding to each level of grid can also be calculated.

There are two methods for the estimation of spatial density eigenvalues. The first method is to combine formulas (8) and (9):

$$num = L/space. \tag{9}$$

The following formula can be obtained:

$$N_i/S_i = N_j/S_j = width/space = \lambda. \quad (10)$$

Therefore, the spatial density eigenvalue is the ratio of the real spatial width of the ocean field to the spatial density coefficient. In this way, when the scale grading is completed, the size of the grid and the number of grid cells at each level can be calculated.

Another method is to adjust the display scale to the adaptive maximum scale. In this state, the solid distance of the grid spacing can be determined. The number of cells in the corresponding grid can be obtained from the field width of the flow field, and the spatial density characteristic value can be obtained according to formula (10).

If the value of the level increment coefficient is too small, it lacks practical significance, and if the value is too large, the data cannot be effectively thinned. Through continuous experiments, the empirical value k of the level increment coefficient is obtained, which is roughly 1.1–1.6. In actual operation, this value can be manually adjusted according to the display accuracy.

$$\begin{aligned} S_i * k &= S_{i+1} \\ N_i * k &= N_{i+1}, k \in [1.1, 1.6]. \end{aligned} \quad (11)$$

In this formula, S_i , S_{i+1} represent the scale at level i, i+1, $V_{\max}$, N_j represent the number of grids at grid level i, j, and k is the level increment coefficient.

The ocean flow field data is divided into regular uniform flow field and irregular flow field according to its spatial distribution characteristics. Since the data elements of the regular flow field and the sparse grid are uniform and regular, the adaptive sparseness processing of the regular flow field data can achieve the uniform adaptive sparse effect by using the idea of the above general algorithm.

Moreover, since each point in the uniform lattice is identified by a unique set of row and column index (i, j), which is convenient for retrieving elements and extracting point sets, the specific operations of sparse processing do not need to generate grids and other data step by step. Moreover, it can easily and quickly retrieve elements in the application and display them. In this paper, ArcEngine is used as the platform for the program implementation of stream field data sparse processing.

The basic idea of the realization of the regular flow field sparse program can be reduced to two transformations. First, the size of the sparse grid is transformed into the problem of "taking a point for every few points" and then transformed into the mathematical law satisfied by the row and column index numbers (i, j), and the qualified point set is searched and retrieved.

The distances between the elements of the flow field data with uniform lattice distribution are equal everywhere, and the cell size of the sparse grid is also the same. Therefore, if it is assumed to be n times of the point spacing, then when superimposed, the number of feature points that fall in the horizontal or vertical direction in the grid cell where the feature points fall is also N. The result of sparse processing is that at most one element point is extracted from each grid unit, so as long as every n points in both horizontal and vertical directions are taken—one element. Its conversion to (i, j) satisfies the condition that i and j are divisible by N at the same time.

Figure 8 shows the situation when the grid cell contains exactly two feature points in the horizontal and vertical directions. At this time, as long as the feature points whose row and column numbers are divisible by 2 are extracted, it is the result of sparseness at the current level.

Based on the basic idea of transforming grid size into index condition, the key to program realization of regular flow field data sparse processing lies in solving the corresponding relationship between grid size and n value. The solution formula is as follows:

$$n = \begin{cases} R/N, R > C \\ C/N, C > R \end{cases}. \quad (12)$$

N is the number of cells in one direction of each grid level. R and C are the number of rows and columns of the regular flow field data lattice, respectively. The adaptive flow field sparse algorithm classifies the scale, and the size of the sparse grid corresponding to each level is usually expressed by the number of grid cells. Since the range of uniform grid division is the smallest circumscribed square of the flow field, the number of cells in each level of grid is equal in the horizontal and vertical directions. Therefore, the size of a pair of grids is expressed as $N \times N$.

The extraction of point sets theoretically requires retrieval control in both horizontal and vertical directions. The number of rows and columns of the regular flow field data lattice is R and C, respectively, but the flow field data with unequal R and C only reach the edge of the minimum circumscribed square in one direction of the horizontal or vertical direction. Therefore, according to formula (13), the grid size of each level is converted into the corresponding n value.

When the user browses the map, the program locates the corresponding level and the n value of the level according to the scale of the current map, queries the elements of the flow field, and obtains the elements whose row and column numbers are divisible by n, which can be seen on the map. The query statement is as follows:

$$[i] \bmod n = 0 and [j] \bmod n = 0. \quad (13)$$

4. Research on Blue Finance of Ocean City Based on GIS

The overall structure of the system is shown in Figure 9. The whole system is divided into data service layer, application service layer, and client application layer from bottom to top. The application service layer consists of two parts: the open-source framework layer and the GIS function service layer. The open-source framework layer is the core framework for data sharing and also provides standard format communication data for the GIS function service layer. The GIS function service layer is the main part of realizing the sharing of ocean data processing service functions, mainly realizing ocean scene modeling, ocean data analysis, and other

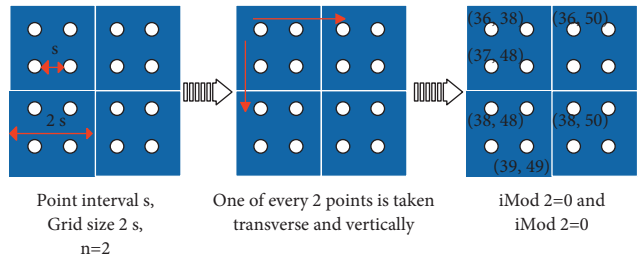

Figure 8: Conversion of grid and retrieval conditions.

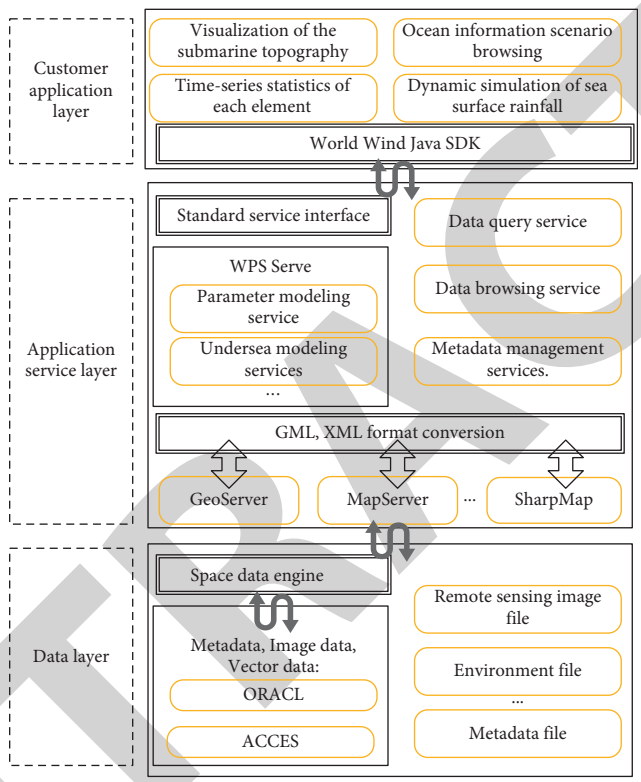

Figure 9: Service-based Web 3D GIS architecture.

services. The client application layer is the interface for the client to realize data browsing and interaction.

The data service layer is the basis for the entire demonstration system to build network application services and is responsible for saving all the data and control information required by the system. According to the characteristics of basic spatial data, data includes not only structured data records, but also unstructured files and image data. For image data, this paper adopts metadata management technology. The multisource, heterogeneous, dynamic, multidimensional, and massive characteristics of ocean environmental comprehensive data determine the complexity of its data management. Moreover, this complexity is reflected in the diversity of data and the complexity of the image vector data itself. According to the sharing requirements of ocean data, the unified interoperability of different data types must be realized. This demonstration system supports a variety of data storage methods. Ocean data can be stored in the form of files or in spatial databases such as Oracle.

The application service layer is the core function layer of the service-based ocean 3D visualization system, including the open-source framework layer and the GIS function service layer. The system is developed on the basis of open-source GIS software to realize operations such as reading multisource ocean data and convert multisource data into standard format communication data to realize network data interoperability. After the open-source GIS framework layer completes data conversion and realizes data interoperability, the GIS function service layer can realize GIS function analysis with standard communication data. The functional interface of the service layer can not only be published in the form of ordinary web service interface, but also follow the WPS specification of OGC to realize the collaborative sharing of multiple GIS functional services. The client application layer mainly realizes the 3D visualization of ocean information, including the visualization of seabed terrain, dynamic simulation of rainfall on the sea surface, simulation of clouds in the sea and sky, and

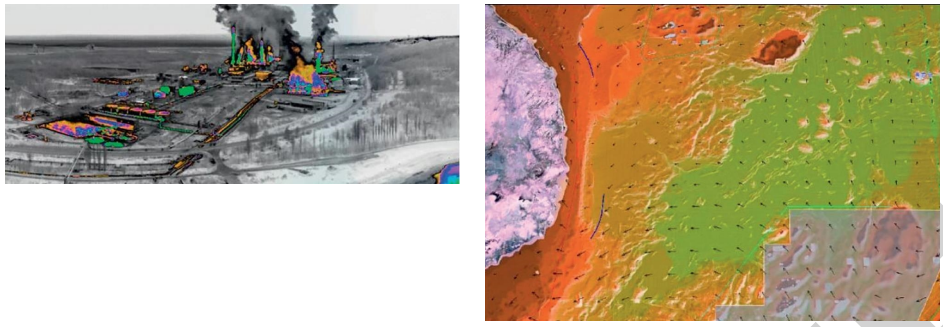

(a) (b)

Figure 10: Simulation of ocean city blue finance based on GIS. (a) Image simulation of coastal economic development (corporate carbon emissions). (b) Ocean climate modeling and its impact on coastal economies.

Table 1: Evaluation of the role of GIS in the development of blue finance in ocean cities.

Number	Test evaluation	Number	Test evaluation	Number	Test evaluation
1	87.25	21	89.19	41	82.25
2	83.43	22	87.20	42	83.57
3	76.59	23	84.13	43	77.19
4	77.75	24	78.46	44	84.40
5	86.72	25	89.35	45	80.67
6	84.83	26	77.16	46	79.79
7	81.15	27	88.76	47	80.73
8	84.37	28	82.14	48	82.68
9	84.47	29	78.38	49	86.57
10	83.21	30	84.05	50	79.52
11	79.44	31	85.06	51	76.18
12	80.65	32	88.96	52	79.20
13	90.01	33	84.53	53	79.05
14	85.61	34	90.73	54	77.20
15	80.21	35	84.40	55	86.40
16	81.63	36	82.27	56	80.05
17	89.48	37	90.91	57	81.61
18	78.90	38	82.47	58	78.13
19	81.00	39	83.68	59	77.69
20	79.44	40	89.53	60	77.92

browsing of ocean scenes. The client calls the application service layer interface to obtain the data information after the analysis and processing of the service layer for rendering and expression of the client. The application layer completes the realization of the application system through the service interface. The client integrates the service interface defined by the application layer and accesses the underlying resources through the protocol of the application layer and no longer needs to care about the complicated and cumbersome implementation mechanism of access. Figure 10 shows an example image of the simulation model in this paper.

On the basis of the above research, the role of GIS in the development of blue finance in ocean cities is explored, and the statistical results are shown in Table 1.

From the above research, it can be seen that the GIS technology proposed in this paper can play an important role in the research of blue finance in ocean cities and has a certain role in promoting the development of ocean blue finance.

5. Conclusion

The ocean provides various resources and environmental support for the development and evolution of human society. The development of the ocean economy must be guaranteed to be sustainable, ensuring the coordinated advancement of the ocean economy, human survival and ecological stability. Moreover, the ocean is an important guarantee for the continuous development and progress of human beings, and without a healthy ocean, the survival of human beings will be difficult to maintain. The ocean economy is an important part of the blue economy, and the development status of the main body of the blue economy will directly affect the development level of the blue economy. Therefore, in order to realize the rapid and healthy blue economy, the ocean economy and ocean related industries will be the focus of development and attention. This paper combines the GIS to carry out the research on the blue

finance of ocean cities, to improve the exploration effect of the development methods of blue finance in ocean cities. The experimental research shows that the GIS technology proposed in this paper can play an important role in the research of blue finance in ocean cities and has a certain role in promoting the development of ocean blue finance.

Data Availability

The experimental data used to support the findings of this study are available from the corresponding author upon request.

Conflicts of Interest

The authors declare that there are no conflicts of interest regarding this work.

References

[1] T. Abou-Chadi and T. Kurer, "Economic risk within the household and voting for the radical right," *World Politics*, vol. 73, no. 3, pp. 482–511, 2021.

[2] T. R. Chowdhury, S. Chakrabarty, M. Rakib, S. Saltmarsh, and K. A. Davis, "Socio-economic risk factors for early childhood underweight in Bangladesh," *Globalization and Health*, vol. 14, no. 1, p. 54, 2018.

[3] E. Asare, A. K. Hoshide, F. A. Drummond, G. K. Criner, and X. Chen, "Economic risk of bee pollination in Maine wild blueberry, Vaccinium angustifolium," *Journal of Economic Entomology*, vol. 110, no. 5, pp. 1980–1992, 2017.

[4] F. Rodriguez, T. Toulkeridis, W. Sandoval, O. Padilla, and F. Mato, "Economic risk assessment of Cotopaxi volcano, Ecuador, in case of a future lahar emplacement," *Natural Hazards*, vol. 85, no. 1, pp. 605–618, 2017.

[5] B. J. Galli and G. Battiloro, "Economic decision-making and the impact of risk management: how they relate to each other," *International Journal of Service Science, Management, Engineering, and Technology*, vol. 10, no. 3, pp. 1–13, 2019.

[6] J. Belás, L. Smrcka, B. Gavurova, and J. Dvorsky, "The impact of social and economic factors in the credit risk management of SME," *Technological and Economic Development of Economy*, vol. 24, no. 3, pp. 1215–1230, 2018.

[7] S. Gangemi, L. Billeci, and A. Tonacci, "Rich at risk: socio-economic drivers of COVID-19 pandemic spread," *Clinical and Molecular Allergy*, vol. 18, no. 1, p. 12, 2020.

[8] N. R. Mosteanu, "Intelligent tool to prevent economic crisis–fractals. A possible solution to assess the management of financial risk," *Calitatea*, vol. 20, no. 172, pp. 13–17, 2019.

[9] J. M. Madsen and J. L. McMullin, "Economic consequences of risk disclosures: evidence from crowdfunding," *The Accounting Review*, vol. 95, no. 4, pp. 331–363, 2020.

[10] Y. B. Chiu and C. C. Lee, "On the impact of public debt on economic growth: does country risk matter?" *Contemporary Economic Policy*, vol. 35, no. 4, pp. 751–766, 2017.

[11] A. R. Safiullin and A. I. Gubaidullina, "Approach to risk and investment attractiveness estimation for regional economic activity of Russia," *International Transaction Journal of Engineering, Management, & Applied Sciences & Technologies*, vol. 9, no. 5, pp. 455–467, 2018.

[12] B. Geetha, C. Sukumar, E. Dhivyadeepa, J. K. Reddy, and V. Balachandar, "Autism in India: a case–control study to understand the association between socio-economic and environmental risk factors," *Acta Neurologica Belgica*, vol. 119, no. 3, pp. 393–401, 2019.

[13] X. Jin, Z. Chen, and X. Yang, "Economic policy uncertainty and stock price crash risk," *Accounting and Finance*, vol. 58, no. 5, pp. 1291–1318, 2019.

[14] M. Swann, "Economic strengthening for HIV prevention and risk reduction: a review of the evidence," *AIDS Care*, vol. 30, no. sup3, pp. 37–84, 2018.

[15] S. Chakrabarti, M. T. Khan, A. Kishore, D. Roy, and S. P. Scott, "Risk of acute respiratory infection from crop burning in India: estimating disease burden and economic welfare from satellite and national health survey data for 250 000 persons," *International Journal of Epidemiology*, vol. 48, no. 4, pp. 1113–1124, 2019.

[16] K. Peng, M. Tian, M. Andersen et al., "Incidence, risk factors and economic burden of fall-related injuries in older Chinese people: a systematic review," *Injury Prevention*, vol. 25, no. 1, pp. 4–12, 2019.

[17] J. E. Laine, V. T. Baltar, S. Stringhini et al., "Reducing socio-economic inequalities in all-cause mortality: a counterfactual mediation approach," *International Journal of Epidemiology*, vol. 49, no. 2, pp. 497–510, 2020.

[18] C. O'Connell, M. Motallebi, D. L. Osmond, and D. L. K. Hoag, "Trading on risk: the moral logics and economic reasoning of North Carolina farmers in water quality trading markets," *Economic Anthropology*, vol. 4, no. 2, pp. 225–238, 2017.

[19] J. Odehnal and J. Neubauer, "Economic, security, and political determinants of military spending in NATO countries," *Defence and Peace Economics*, vol. 31, no. 5, pp. 517–531, 2020.

[20] K. Broekhuizen, D. Simmons, R. Devlieger et al., "Cost-effectiveness of healthy eating and/or physical activity promotion in pregnant women at increased risk of gestational diabetes mellitus: economic evaluation alongside the DALI study, a European multicenter randomized controlled trial," *International Journal of Behavioral Nutrition and Physical Activity*, vol. 15, no. 1, p. 23, 2018.